PAPER

Plasma current asymmetries during disruptions in JET

IOP Publishing | International Atomic Energy Agency Nuclear Fusion
Nucl. Fusion **54** (2014) 073009 (14pp) doi:10.1088/0029-5515/54/7/073009

Plasma current asymmetries during disruptions in JET

S.N. Gerasimov[1], T.C. Hender[1], J. Morris[1], V. Riccardo[1], L.E. Zakharov[2] and JET EFDA Contributors[a]

JET-EFDA, Culham Science Centre, OX14 3DB, Abingdon, UK
[1] Euratom/CCFE Fusion Association, Culham Science Centre, OX14 3DB, Abingdon, UK
[2] PPPL, Princeton University, Princeton, NJ 08543, USA

E-mail: Sergei.Gerasimov@ccfe.ac.uk

Received 13 June 2013, revised 10 March 2014
Accepted for publication 10 March 2014
Published 23 April 2014

Abstract

A key feature of disruptions during vertical displacement events, discovered in JET in 1996, is the toroidal variation in the measured plasma current I_p, i.e. the plasma current asymmetries, lasting for almost the entire current quench. The unique magnetic diagnostics at JET (full set of poloidal coils and saddle loops recorded either from two toroidally opposite or from four toroidally orthogonal locations) allow for a comprehensive analysis of asymmetrical disruptions with a large scale database. This paper presents an analysis of 4854 disruptions over an 18 year period that includes both the JET carbon (C) wall and the ITER-like (IL) wall (a mixed beryllium/tungsten first wall). In spite of the I_p quench time significantly increasing for the IL-wall compared to C-wall disruptions, the observed toroidal asymmetry time integral ($\sim$ sideways force impulse), did not increase for IL-wall disruptions. The I_p asymmetry has a dominantly $n = 1$ structure. Its motion in the toroidal direction has a sporadic behaviour, in general. The distributions of the number of rotation periods are found to be very similar for both C- and IL-wall disruptions, and multi-turn rotation was sometimes observed. The I_p asymmetry amplitude has no degradation with rotation frequency for either the C- or IL-wall disruption. Therefore dynamic amplification remains a potentially serious issue for ITER due to possible mechanical resonance of the machine components with the rotating asymmetry.

Keywords: tokamak, disruption, VDE, kink instability, plasma current asymmetries

(Some figures may appear in colour only in the online journal)

1. Introduction

Disruptions remain a critical issue for any scenario operation of ITER [1]. Electro-magnetic loads, heat loads and runaway electron generation are the main concerns of disruption impacts on the machine components [2]. In addition to the plasma boundary reconstruction, JET magnetic diagnostics are capable of extracting the toroidal asymmetries in the plasma current (I_p) and the vertical and radial components of the plasma displacement. It is evident on JET that toroidal asymmetries during vertical displacement events (VDEs) can lead to substantial sideways forces of up to about 4 MN [3–6], and in turn cause significant displacements of the JET torus [3]. These 'VDE' forces are expected to increase for larger machines such as ITER. The sideways force F_x and vertical force F_z on the vessel are estimated to be an order of magnitude larger in ITER in comparison with JET [5–8]. This also follows from simple dimensional analysis: $F_x \propto B_T I_p a$, $F_x^{ITER} \cong 2 \cdot 5 \cdot 2F_x^{JET} \cong 20F_x^{JET}$; $F_z \propto I_p^2$, $F_z^{ITER} \cong 5^2 F_z^{JET} \cong 25F_z^{JET}$, where B_T, a are toroidal field and plasma minor radius respectively. This estimation assumes that JET and ITER have similar plasma shape, plasma profiles, mode structure and relative asymmetry amplitude. Detailed engineering analysis confirms the order of magnitude increase of these forces for ITER [9]. Apart from the force itself, the force impulse ($\int F_x \, dt$) and force time behaviour are important for the vessel structural loads. The rotation of asymmetries is an important effect of the disruptions on the vacuum vessel deformation. Besides the sporadic rotating asymmetry in the plasma current I_p, found on JET [5, 8], a similar effect of rotation of the asymmetrical halo current structures (measured by different halo current diagnostics) was observed on JT60-U [10], Alcator C-Mod [11], DIII-D [12], ASDEX-U [13] and NSTX [14, 15]. While many other tokamaks have halo current diagnostics no other tokamak apart from JET has published results on plasma current asymmetries during disruptions.

Frequencies that are close to the structural natural frequencies of the machine components can cause major dynamic amplifications of the loads. For the ITER vessel the most problematic rotation frequency is $\sim$3–8 Hz, which is in the range of the fundamental mechanical vessel frequencies [16].

[a] See the appendix of Romanelli F. *et al* 2012 *Proc. 24th IAEA Fusion Energy Conf. 2012 (San Diego, CA, 2012)* (www-naweb.iaea.org/napc/physics/FEC/FEC2012/index.htm).

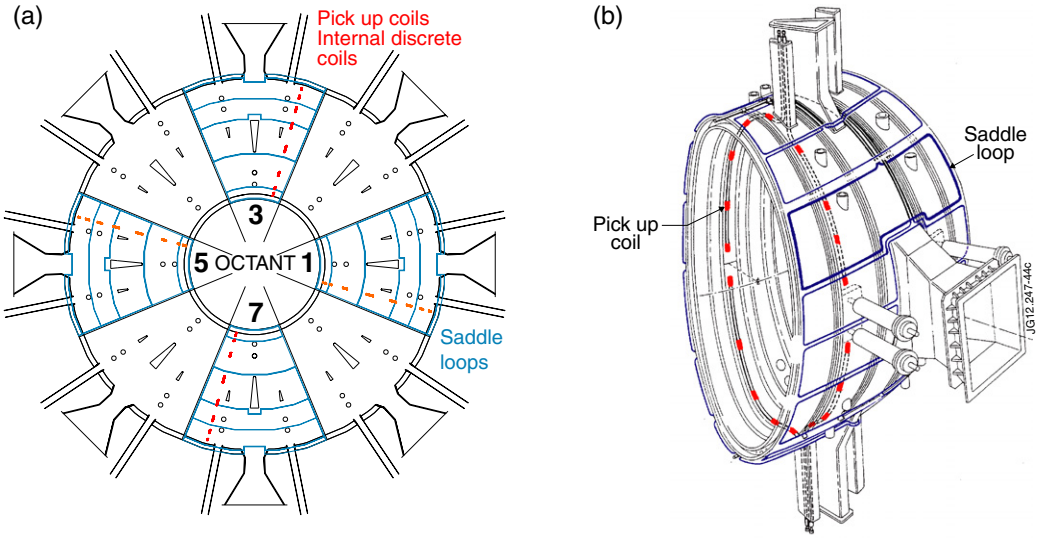

Figure 1. (*a*) Plan view of JET vessel, showing the toroidal locations of the pick-up coils and saddles. (*b*) JET vessel octant equipped with pick-up coils (named IDC) and saddle loops.

JET magnetic diagnostics, which are essential for the presented results, are described in section 2. The composition of the plasma current asymmetry database is given in section 3. The I_p, M_{IZ} asymmetries and poloidal field (PF) variation structures observed during VDEs are outlined in section 4. Plasma current asymmetries, sideways forces and impulses data, which were extracted from 4854 disruptions over an 18 year period of JET operation, are detailed in section 5. The rotation of the plasma current asymmetries is discussed in section 6. Possible physical interpretations are sketched in section 7. Remaining issues, which are the subject of future investigations, are discussed in section 8. The results of the disruption analyses in terms of plasma current asymmetries are summarized in section 9.

2. Diagnostics

On JET toroidal asymmetries of the plasma current (I_p) and its moments ($M_{IZ} \equiv \int Z J_\phi \, dR \, dZ$ and $M_{IR} \equiv \int (R - R_o) J_\phi \, dR \, dZ$ [20]) are measured using arrays of in-vessel tangential poloidal pick-up coils (named internal discrete coils, IDC) and ex-vessel normal saddle loops at four orthogonal toroidal locations (see figure 1). Each octant is equipped with 18 pick-up coils and 14 saddle loops.

The plasma current is calculated using the following equation (Ampere's law $\mu_0 I = \oint \vec{B} \, \overrightarrow{dl}$ that is adapted to JET conditions, I is total toroidal current inside the measuring contour):

$$I_p = \frac{1}{\mu_0} \sum_{i=1}^{18} B_{\vartheta i} d_i - \sum_{i=1}^{4} n_{Di} I_{Di} - (I_{\mathrm{RRU}} + I_{\mathrm{RRL}}), \qquad (1)$$

where $B_{\vartheta i}$ is the poloidal (tangential) field measured by the ith IDC, d_i is the length of the relevant arc. The last two terms are the axisymmetric currents occurring inside the measuring contour (which are identical for all octants), where $\sum_{i=1}^{4} n_{Di} I_{Di}$ are the currents in divertor PF coils and (I_{RRU}+I_{RRL}) are the currents in the restraining rings, which are toroidally continuous conducting structures. Restraint rings were installed in 1988 to reduce the deformation of the vessel during disruptions at high current [21]. Equation (1) does not include the axisymmetric currents in the divertor support structure and divertor PF coil cases (I_{MK2}) because reliable measurements are not available for all pulses in the presented database. The amplitude of the induced I_{MK2} could be up to 5% of pre-disruptive plasma current for fast current quench (CQ). However the axisymmetric I_{MK2} current does not affect the toroidally asymmetrical part of the plasma current.

The first plasma current vertical moment is calculated using the equation (the derivation of general $M_{IZ} = \int Z J_\phi \, dR \, dZ$ expression for JET environment):

$$M_{IZ} = \frac{1}{\mu_0} \left(\sum_{i=1}^{18} B_{\vartheta i} z_i d_i + \frac{1}{2\pi} \sum_{i=1}^{14} \Psi_i \ln \left(\frac{R_o}{r_i} \right) \right) - \sum_{i=1}^{4} z_{Di} n_{Di} I_{Di} - (z_{\mathrm{RRU}} I_{\mathrm{RRU}} + z_{\mathrm{RRL}} I_{\mathrm{RRL}}), \qquad (2)$$

where Ψ_i is the flux measured by ith saddle, z_i and r_i are IDCs and saddle coil coordinates, z_{Di} and $z_{\mathrm{RRU/L}}$ are the coordinates of the divertor coils and restraining rings respectively. The divertor support structure and divertor PF coil contributions were not taken into account in equation (2), see previous explanation for equation (1). It is worth mentioning that the current centroid position does not reflect the true geometrical plasma boundary position in the case of asymmetrical surface currents or, in other words, 3D equilibrium.

The pick-up coil and saddle signals are processed by analogue low-drift integrators with a 16-bit analogue to digital converter. The data is recorded at a 5 kHz sampling rate during the whole JET pulse or, at least, during the disruption time window. Data for octants 3 and 7 has been recorded from shot #32102 (15/10/1994) onwards. Additionally two octants 1 and 5 have been recorded regularly from shot #64329 (03/11/2005) onwards, allowing I_p asymmetry amplitude and phase to be deduced.

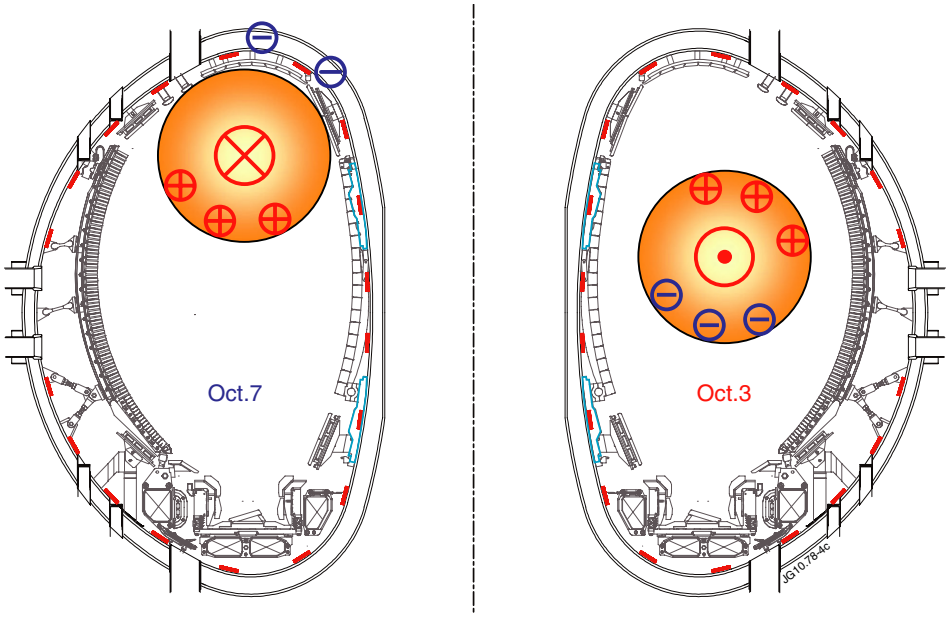

Figure 2. JET vessel cross-section and measured I_p asymmetry explanation. Negative surface plasma current flows on vessel in octant 7 and bypasses IDC contour. Restraining ring ribs are shown in light blue.

All 8 JET octants were originally equipped with identical sets of IDCs and saddles (with some minor exceptions for 3 and 7 octants). Later on, the 9 upper IDCs were removed from octant 8 to allow the installation of another diagnostic. The whole data set from the IDCs and saddles in octants 2, 4, 6 and 8 were not recorded, and because of this they are not used in the analysis.

There are two toroidal in-vessel passive structures, which can affect the interpretation of the IDCs measurements. They are the restraining rings and the divertor support structure/divertor coil cases, figure 2. Two of the IDCs (coils 8 and 11) are located between the vessel and the restraining rings. The vessel current can flow through the restraining rings and affect the local measurements of coils 8 and 11. Coils 8 and 11 are effectively located outside the vessel current circuit while the rest of the coils (excluding coils behind the divertor structure, see comments below) are located inside the vessel current circuit. Figure 3 shows the PF subtracted on 2 opposite sides of the torus (octant 7–octant 3), during an upward VDE. The change of sign of the PF in figure 3 with time is due to rotation of the I_p asymmetry. It can be seen by inspection that the field at coil 8 has an opposite sign to that expected by simple interpolation between coils 7 and 9, and likewise for coil 11. It is thought this change in sign is caused by currents flowing in the vessel restraining ring, between the coil and plasma. To assess the impact of this on the calculated plasma current, the signal in coil 8 has been replaced by an average of the signals from coils 7 and 9, and the coil 11 signal has been replaced by an average of coil 10 and 12. This procedure indicates that the shielding effect produces up to a ∼15% underestimate of the asymmetric current and vertical moment calculated by (1) and (2). At least three IDCs (13, 14 and 15 coils) are positioned between the vessel and divertor passive structure. Hence, for downward VDEs the magnetic measurement interpretation suffers due to the uncertainty of the current passive structure circuits.

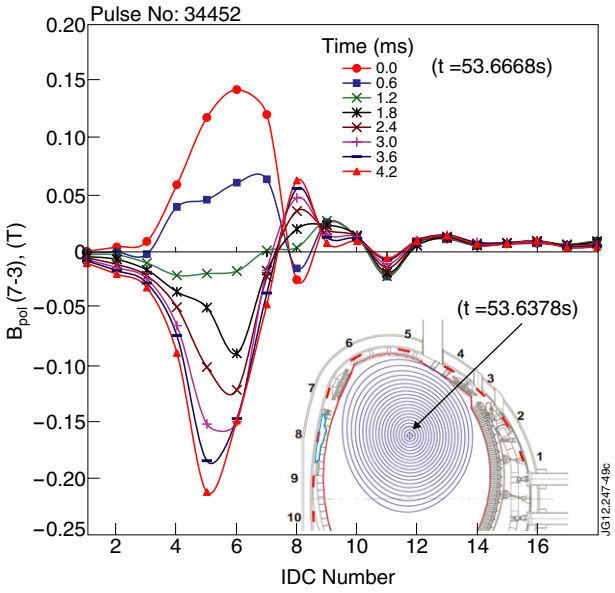

Figure 3. The asymmetry of the PF measurements from IDCs. The insert shows the coil locations in the upper vessel (coils 10 to 18 are a mirror image); equilibrium reconstruction just before rise of the I_p asymmetry; restraining ring rib is shown in light blue.

3. Plasma current asymmetry disruption database

The presented JET disruption database includes pulses, where $I_p^{dis} > 1.0$ MA (I_p^{dis} is pre-disruptive plasma current, defined as the average I_p over 20–50 ms before the disruption time, T_{dis}), for all cases, not just VDEs. In the results presented the time of disruption is defined as the moment when $|dI_p/dt| > 25\,MA\,s^{-1}$ for at least 2 ms or as the time of the peak of the voltage loop spike (>10 V). Manual checks and minor corrections (where necessary) were applied to the entire database. Some of the disruptions exhibit multiple plasma

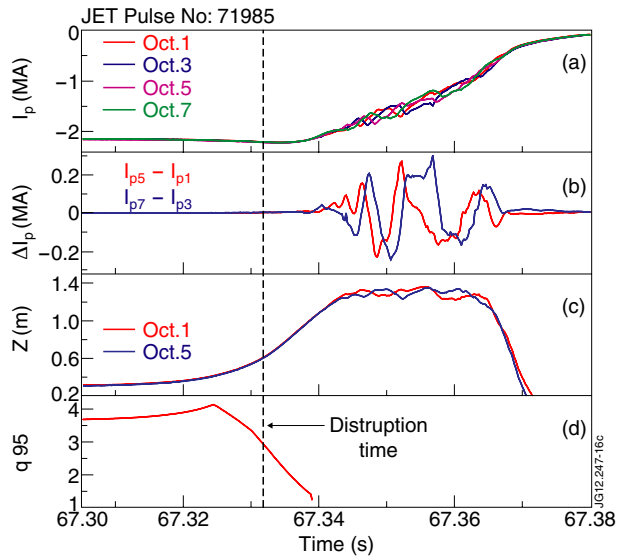

Figure 4. Waveforms of the measured asymmetries: (*a*) plasma currents, (*b*) I_p asymmetries, (*c*) vertical plasma current centroid displacements and (*d*) q_{95} edge safety factor. The vertical dashed line indicates the disruption time.

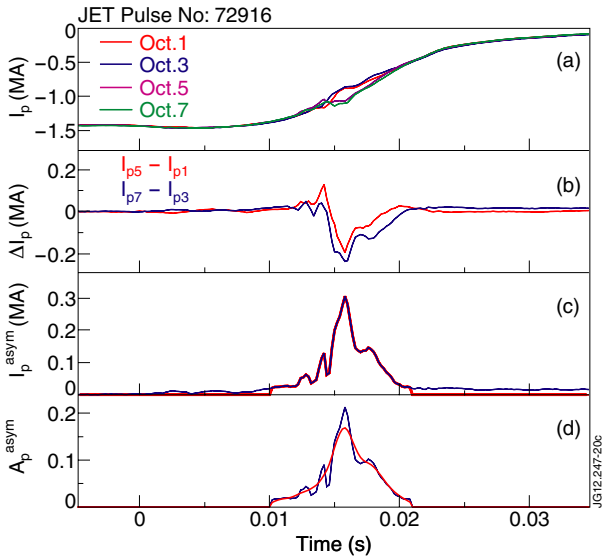

Figure 5. Waveforms of the measured asymmetries: (*a*) plasma currents, (*b*) I_p asymmetries, (*c*) amplitude of the I_p asymmetries (blue—original, red—trimmed), (*d*) normalized amplitude of the I_p asymmetries (blue—trimmed, red—smoothed). The time axis is normalized to T_{dis}.

current spikes, where the first event is treated as the start of the disruption. The above algorithm provides a disruption time just before the plasma current spike followed by plasma CQ or a disruption time just before plasma CQ for VDE disruptions. The plasma current asymmetry analysis is not affected by the somewhat arbitrary choice of the disruption time.

The database includes 4854 (unplanned, or intentional as part of a disruption study) disruptions in the range #32102–#83794, which covers a period of JET operation from 15/10/1994 to 27/07/2012. During this period, 1300 disruptions have been recorded using 4 octants, which have been used for rotation analysis. The pre-disruptive plasma current and toroidal field are in the range 1.0–4.6 MA and 0.6–3.8 T respectively for the entire database.

Replacement of carbon plasma-facing components (referred to here as JET 'C-wall') by solid beryllium limiters and beryllium tiles in the main chamber, and a combination of bulk W and W-coated divertor tiles (referred to here as JET 'ITER-like (IL)-wall') was completed on JET in 2011 [22–25]. The presented C-wall I_p asymmetries rotation (4 octants) database contains 951 shots. The C-wall database also contains 3490 pulses of two-octant disruption data, which has been used for non-rotational analysis only. The whole IL-wall current database contains 413 disruptions out of which 349 are recorded using 4 octants and 64 are recorded in 2 octants only, because of the data acquisition system (DAS) faults or insufficient duration of the 5 kHz window in one of the magnetics DAS. Figure 4 shows the waveforms of the typical asymmetrical VDE disruption before and during a plasma CQ, where plasma current asymmetries are $\Delta I_{p73} = I_{p7} - I_{p3}$ and $\Delta I_{p51} = I_{p5} - I_{p1}$ with I_{p1} = octant 1 plasma current etc. In the limited number of cases examined, the I_p asymmetries usually appear when the q safety factor drops to 1 because the large plasma vertical displacement during VDE causes the minor plasma radius decrease at approximately constant I_p.

The amplitude of the plasma current asymmetries is calculated as $I_p^{asym} = \sqrt{(I_{p7} - I_{p3})^2 + (I_{p5} - I_{p1})^2}$. In the case when only the two-octant measurements were available the amplitude plasma current asymmetries were calculated as $I_p^{asym} = \sqrt{(I_{p7} - I_{p3})^2}$ or $I_p^{asym} = \sqrt{(I_{p5} - I_{p1})^2}$ [5]. The other quantity which has been used, is the normalized amplitude $A_p^{asym} = I_p^{asym}/|I_p^{dis}|$. To avoid noise contributing to the results, A_p^{asym} is evaluated for times when the start and end time window satisfied the following conditions: $A_p^{asym} > 0.5\%$, $|I_p| > 0.1|I_p^{dis}|$ and $|I_p^{asym}| > 20$ kA for the first and last 1 ms window in order to disregard short-lived spikes. The A_p^{asym} values that do not satisfy the criteria are treated as noise and forced to zero, in other words the waveforms are trimmed. The above defined time window was applied for all other waveforms, which have been used for analysis.

Under the previously developed ITER specification [28] a ±2 ms triangular smoothing of the JET data was applied, on the basis that such short timescale behaviour (when extrapolated to ITER) will have no mechanical effects. Given the ~3–8 Hz ITER vessel frequency the choice of ±2 ms smoothing time (though somewhat arbitrary) is conservative. The triangular smoothing function can be described by the general expression:

$$S(t) = \int_{t-\zeta}^{t+\zeta} Y(s)w(s)\,\mathrm{d}s,$$

$$\text{where } w(s) = \begin{cases} (s - t + \zeta)/\zeta, & t - \zeta \leqslant s \leqslant t \\ (t - s + \zeta)/\zeta, & t \leqslant s \leqslant t + \zeta, \end{cases}$$

where ζ is half width of the smoothing interval, $Y(t)$ is original function and $S(t)$ is smoothed function.

The maximum of the presented quantities in this paper were chosen from the smoothed waveforms to ignore the short-lived outliers. Figure 5 shows an example of the plasma current asymmetries at the different stages of the numerical processing: I_p^{asym}—amplitude of the asymmetries (peak to peak, original and then trimmed), A_p^{asym}—normalized asymmetry amplitude (trimmed and smoothed).

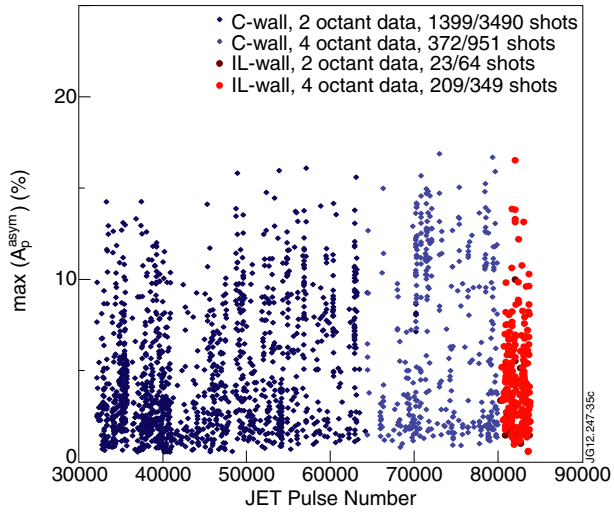

Figure 6. The amplitude of smoothed I_p asymmetry is $<\sim$17% of pre-disruptive I_p for whole range of the recorded disruptions.

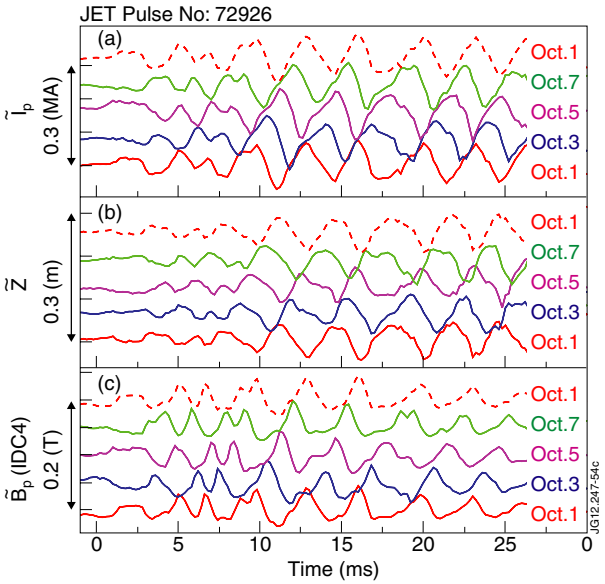

Figure 7. The variations of the plasma current, vertical displacement of plasma current centroid and PF around the torus show that I_p asymmetry is $n = 1$ dominated. (*a*) plasma current, (*b*) vertical displacement of plasma current centroid, (*c*) IDC 4 PF. The time axis is normalized to T_{dis}.

The peak values of A_p^{asym}, extracted from smoothed waveforms, are plotted in figure 6. The 4-octant data presents the true magnitude of the asymmetries. On the other hand two octant data, in general, can underestimate the amplitude for asymmetries which are orthogonal to diagnostics. The fractions on the figure indicate the share of the disruptions that are treated as asymmetrical disruptions; only the asymmetrical disruptions are plotted. The rest of the disruptions are treated as symmetrical disruptions because the level of asymmetry is below the 'noise' level. The total fraction of asymmetrical disruptions in the presented database is $0.41 = 2003/4854$, where the C-wall asymmetrical disruption fraction is $0.40 = 1771/4441$ and the IL-wall fraction is $0.56 = 232/413$. The boundary of the normalized I_p asymmetries $A_p^{asym} \approx 17\%$ is about the same for whole range of 4854 disruptions.

To systematically quantify the magnitude of I_p asymmetries the integral $A = \int A_p^{asym}\,dt$ has been used. Ignoring transients $A \sim \int F_x\,dt/I_p B_T a$, where F_x is the asymmetric (or sideways) force. So A is related to the magnitude of the sideways force impulse; it should be noted that A represents the modulus of the impulse and not a projection in a specific direction. Of the asymmetrical disruptions, the majority (76%) are upward going VDEs. Moreover, the most severe observed asymmetrical disruptions ($A > 0.2A_{max}$) and almost all disruptions (99%) result in upward going VDEs.

4. I_p asymmetry structure

As discussed in detail below (section 6) the I_p asymmetry structure can rotate toroidally. This rotation allows one to examine the spatial structure of the asymmetry. Figure 7 shows the waveforms of plasma current, vertical current centroid position and PF, at 4 toroidal locations separated by 90°: here $\tilde{x}(j) = x(j) - \langle x(j)\rangle$, where $x(j)$ is the value at the j-octant and $\langle x(j)\rangle$ is an average for the four octants. The change of $\tilde{I}_p$ with time, is due to the rotation of the asymmetric component of the plasma current, and can be seen to have a $n = 1$ dominated toroidal structure. However, a $n = 2$ structure can be seen in range from 0 to 5 ms in figure 7. The temporal and spatial variation of plasma current centroid is consistent with a $n = 1$ kink displacement (though its value could be affected by asymmetrical plasma surface currents). Finally the variation of $\tilde{B}_p$ in space and time, will be partly due to the rotating vessel current (experimentally observed as plasma current asymmetry) and partly due to the plasma kink. Likewise figure 8 shows the poloidal variation of $\tilde{B}_p$ at octant 3 and octant 7. The variation of poloidal magnetic field structure can be seen to be dominantly $m = 1$ mode. As with the pulse shown in figure 4, equilibrium reconstructions show that edge-q approaches 1 at the time when the I_p asymmetries start. These results confirm the dominant $n = 1$ character of the I_p asymmetry and that I_p asymmetry could be associated with the $m = n = 1$ mode. Nevertheless, other poloidal and toroidal harmonics are clearly superimposed to the $m = n = 1$ structure during the whole time interval shown. Further interpretation will require comparison of the experimental results with appropriate dynamic plasma simulations to unambiguously separate the effects of spatial variations of currents in the plasma and vessel, from the kink distortion of the plasma.

The phase relationship of the measured I_p and first vertical plasma current moment (M_{IZ}) is a discriminator for models of the wall currents. Figure 9 shows the typical waveforms (I_p, ΔI_p, ΔM_{IZ} and ΔZ) during the plasma CQ. The measured absolute magnitude of the plasma current is greater when displacement is also greater [3, 4, 5, 7]. Specifically, the toroidal asymmetry in plasma currents corresponds to negative currents (relative to the direction of plasma current) flowing in the vessel as shown by the I_p and M_{IZ} asymmetries phase diagram, where ΔI_{p73} plotted versus $\Delta M_{IZ73} = M_{IZ7} - M_{IZ3}$ and ΔI_{p51} plotted versus $\Delta M_{IZ51} = M_{IZ5} - M_{IZ1}$ (figure 10). The fractions in figure10 present the share of the disruptions which were used for the plot. The remainder

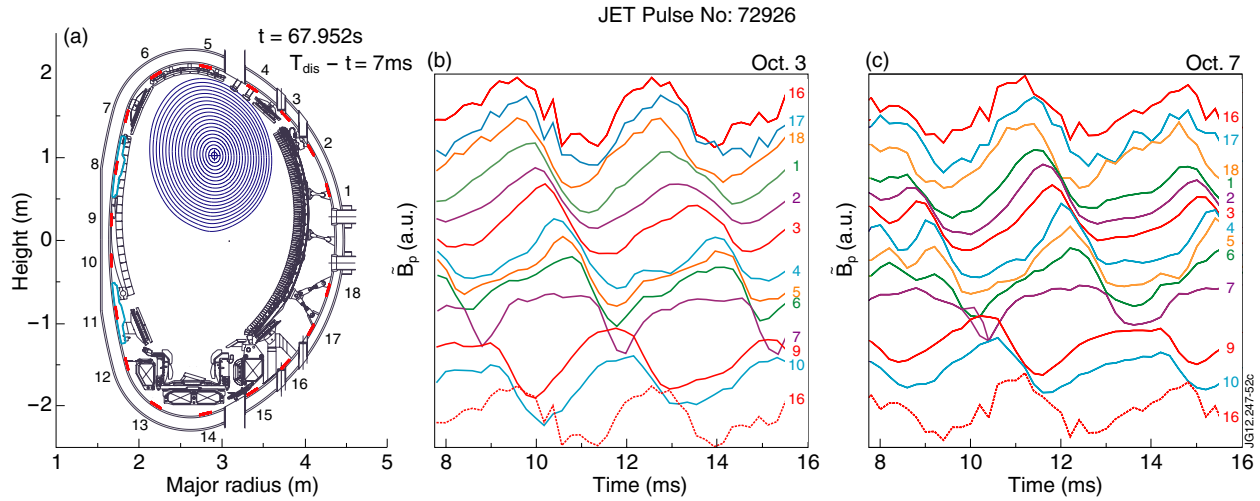

Figure 8. (*a*) Equilibrium reconstruction just before rise of the I_p asymmetry; numbers show the IDCs. PF oscillations at octant 3 (*b*) and octant 7 (*c*) showing a dominantly $m = 1$ variation. The IDC numbers are indicated next to each waveform, the time axis is normalized to T_{dis} and the $\tilde{B}_p(j)$ amplitudes are normalized with respect to each other.

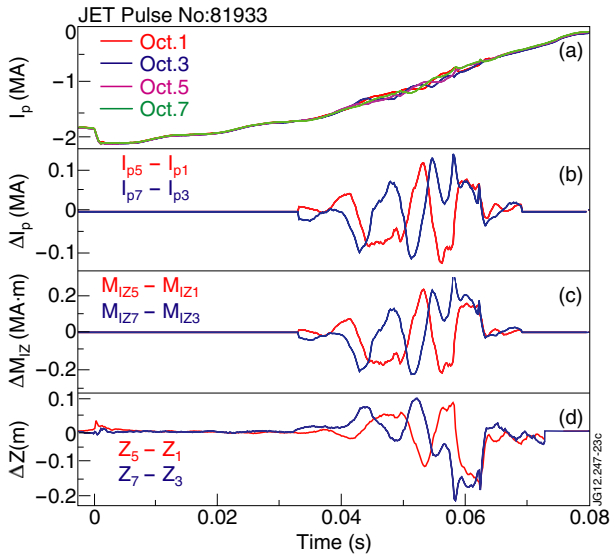

Figure 9. Waveforms of the measured asymmetries: (*a*) plasma currents, (*b*) I_p asymmetries, (*c*) M_{IZ} asymmetries, (*d*) asymmetries of the vertical current centroid displacement. The time axis is normalized to T_{dis}.

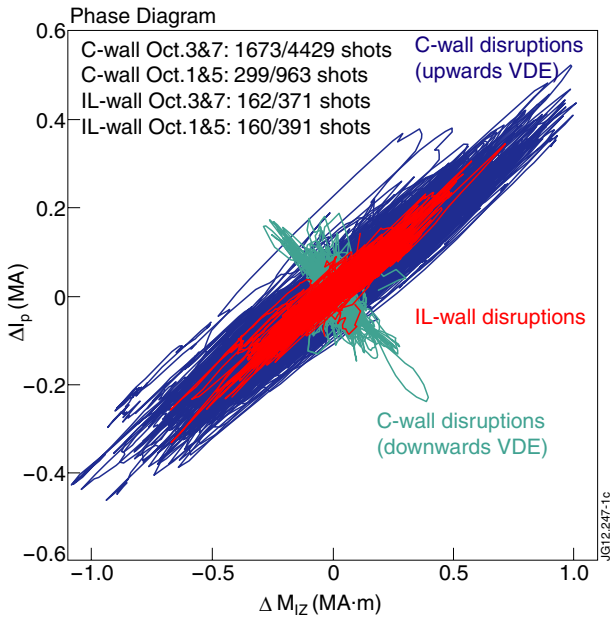

Figure 10. Phase relationship of the I_p and M_{IZ} asymmetries (where ΔI_p presents ΔI_{p73} and ΔI_{p51}, and ΔM_{IZ} presents ΔM_{IZ73} and ΔM_{IZ51}): greater displacement leads to greater measured I_p asymmetry. The downwards VDE trajectories are orthogonal to upwards VDE trajectories because of the displacement polarity.

of the disruptions were below 'noise' level (see previous definition for 'noise'). The sign of the observed asymmetry corresponds to the predictions of the Wall Touching Kink Mode theory [7, 18, 34] as well as to simulation with M3D code [26]. Further interpretation of JET experimental results will require comparison with appropriate simulations.

5. Plasma current asymmetries, sideways forces and impulses

The variation of $A(A_{4oct}\text{or}A_{2oct}) = \int A_p^{asym}\,dt$ over the disruption database is plotted in figure 11. In cases where only two opposite octant data were available a 2-octant asymmetry was defined assuming a pure sine wave in time $A = \pi A_{2oct}/2$ (generally $\pi A_{2oct}/2$gives a good approximation of the 4-octant data). This is shown in figure 12, where for shots with 4 octant data the value of A_{4oct} is compared against $\pi A_{2oct}/2$. It can be seen that on average $\pi A_{2oct}/2$ is a good approximation, however A_p^{asym} does not vary sinusoidally in general and so there is some scatter. The probability that a certain value of A is reached can be inferred from figure 13. The largest I_p asymmetries correspond to upward moving VDEs—quantified by A the largest 17.6% are all upward going VDEs. All the specific time histories of pulses shown in this paper are for upward moving VDEs.

The database contains results for the C-wall and IL-wall—it is known that the wall material strongly affects the disruption

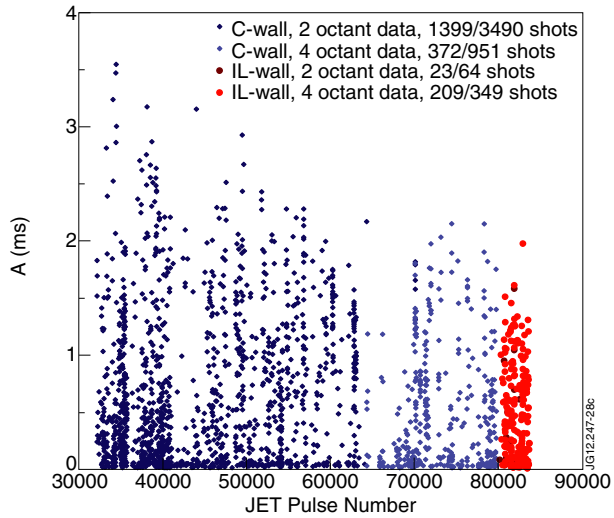

Figure 11. The integral of normalized I_p asymmetries for the entire disruption database.

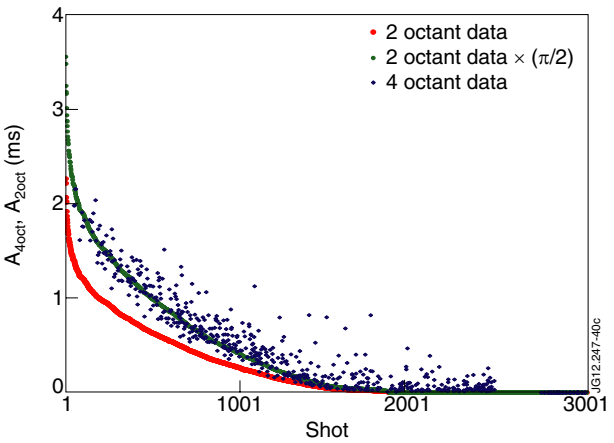

Figure 12. The entire 2 octant database (red), data for 4 octant shots (dark blue) where it exists, and $\pi A_{2\mathrm{oct}}/2$ (green)—the data are sorted by descending size of $A_{2\mathrm{oct}}$.

due to impurity radiation during the CQ [29–31]. There is a significant difference in the current decay for C-wall and IL-wall disruptions. In figure 14 the normalized plasma current for all IL-wall disruptions (figure 14(*a*)) and for a 951 pulse (4 octant data) subset of the C-wall disruptions (figure 14(*b*)) shows substantially longer CQ times for IL-wall disruption. The entire disruption database demonstrates that the CQ time distribution for IL-wall is broader and generally shifted to longer decay times in comparison with C-wall [8], see figure 14(*c*). Moreover, a large fraction of IL-wall disruptions last for hundreds of milliseconds. This occurs because the CQ duration relates to the L/R (inductance/resistance) time of the plasma. In the IL-wall plasma, the temperature during disruption is higher than in C-wall plasma due to the absence of carbon [22, 27]. The CQ time is also affected by VDE dynamics.

Despite the longer IL-wall CQ times the sideways impulse measured by A does not increase. This is illustrated in figure 15 which shows that IL-wall I_p asymmetry data points are inside the C-wall domain. The data boundaries for the whole CQ duration are:

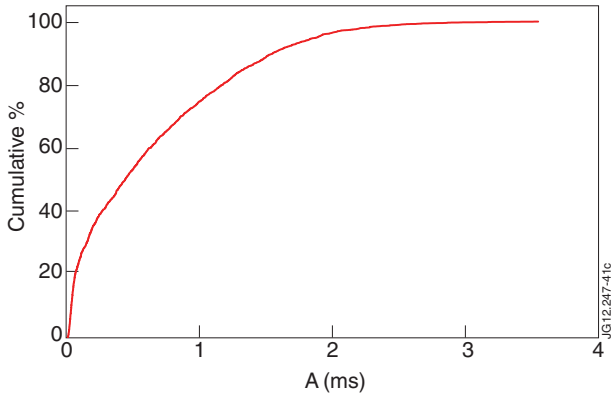

Figure 13. Cumulative % of shots with A less than a given value.

- $A = 0.10\tau_{80-20}$ with $A_{\max} = 3.5$ ms for the C-wall data (green lines);
- $A = 0.06\tau_{80-20}$ with $A_{\max} = 2.0$ ms for the IL-wall data (magenta lines).

It is thought that the comparison of IL-wall data should be made with recent C-wall data because of the JET power supply upgrade, improvement of discharge shutdown etc. The recent C-wall disruptions (4 octant data, pulses in the range 64329–79831) and the IL-wall data have about the same boundary (magenta lines in the figure 15). The plasma CQ time distributions for three thresholds of the I_p asymmetry integral (A) are shown in figure 16. It can be seen that I_p asymmetrical disruptions have a mode (maximum value of a distribution) CQ duration about two times longer for IL-walls in comparison with C-wall disruptions (from #64329 onwards). The CQ duration for severest IL-wall asymmetrical disruption does not exceed 130 ms, whereas the symmetrical disruptions could be ten times longer.

In an integral sense the $A_{\max}$ on figure 15 give the bounding values. However if a trapezoidal envelope for A_p^{asym} is fitted then larger values are needed; the traces of A_p^{asym} for the C-wall and IL-wall disruptions with largest values of A ($A_{4\mathrm{oct}}$ or $A_{2\mathrm{oct}}$) are shown in figures 17, 18 and 19. Figures 17 and 19 present the severest disruptions from the whole C-wall and IL-wall data, respectively. Figure 18 shows recent C-wall 4 octant data. In these plots $t = 0$ is defined such that $\int_{t<0} I_p^{\mathrm{asym}}\,\mathrm{d}t = \int_{t>0} I_p^{\mathrm{asym}}\,\mathrm{d}t$. A trapezoidal shape of envelope has been chosen below to illustrate the relation of the severest asymmetries for the C-wall (whole and 4 octant subset data) and the IL-wall. The choice of the shape and area of envelopes are rather arbitrary but we believe it improves the presentation of the experimental data. Other waveforms of the envelope could be chosen: e.g. a square envelope has been used in [9]. As can be seen by visual inspection the trapezoidal envelope with an area of 3.5 ms, does not bound the observed A_p^{asym} waveforms, figures 17 and 18. A conservative choice would be 4.4 ms and a very conservative choice would be 6.3 ms for C-wall disruptions. The IL-wall disruptions are also well bounded by C-wall disruption envelopes, figure 19. The application of the JET plasma current asymmetry results to ITER was discussed in [9].

The sideways force can be evaluated using Noll's formula [3], $F_x^{\mathrm{Noll}} = \frac{\pi}{2} B_T \Delta M_{IZ}$, which gives the upper estimation

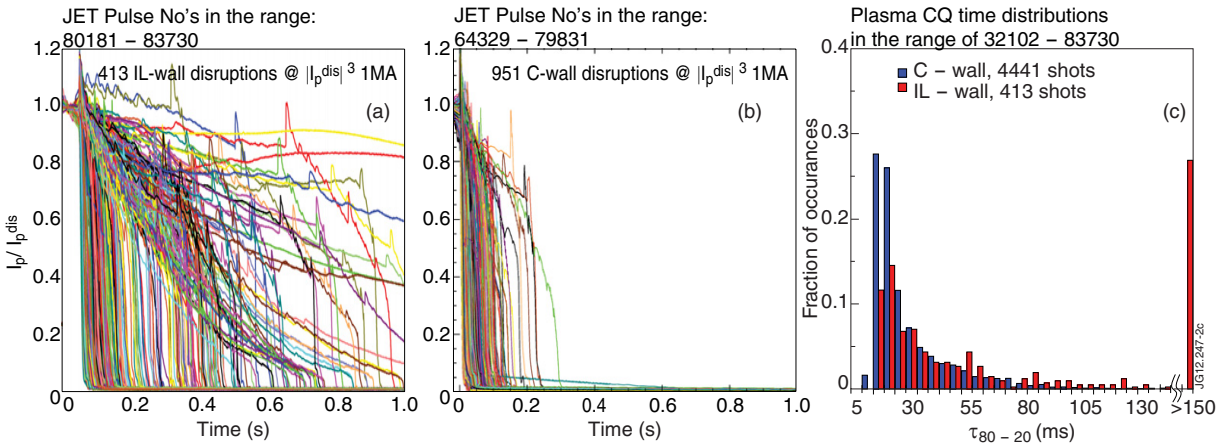

Figure 14. Normalized plasma current during disruptions: (*a*) IL-wall, (*b*) C-wall (only 951 last disruptions are shown) and (*c*) their CQ time distributions for entire database; where τ_{80-20} is the CQ time extrapolated from the time taken to quench from 80% to 20% of I_p^{dis}.

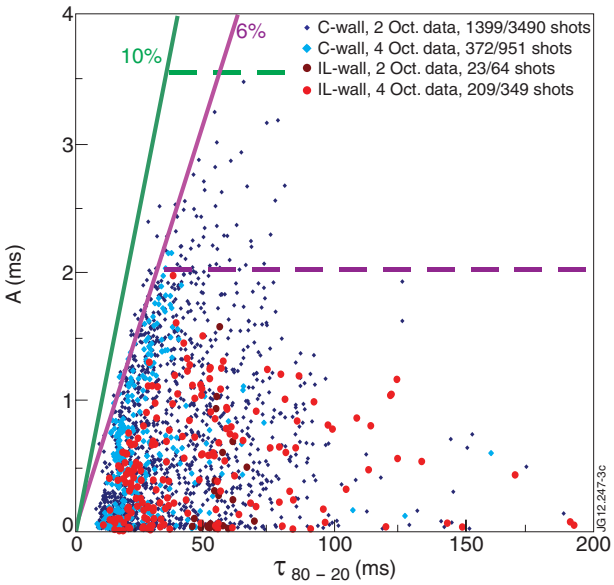

Figure 15. The severity of I_p asymmetries for C- and IL-walls.

for sideways force [18]. The advantage of the Noll's formula is that it includes quantities which are directly measured by magnetic diagnostics, see for example figure 20. Both quantities, I_p^{asym} and $F_x^{Noll} = \frac{\pi}{2} B_T \Delta M_{IZ} \propto B_T I_p^{asym} a$, can be used to characterize peak loads during asymmetrical disruptions. Figure 21 shows the variation of the sideways force impulse evaluated using Noll's formula $\mathrm{Imp}^F = \int F_x^{Noll}\, dt$ for the disruption database, where $F_x^{Noll}$is the force modulus.

The sideways force impulse can also be deduced from the plasma current asymmetry: $\mathrm{Imp}^A = \pi B_T \langle a \rangle \int I_p^{asym}\, dt = \pi B_T \langle a \rangle I_p^{dis} A$, where $\langle a \rangle$ is the average plasma minor radius. The plasma minor radius was taken from EFIT reconstruction just before disruption in the time window [T_{dis}—0.1 s: T_{dis}] or was taken as $\langle a \rangle = 1.205$ m (average data) if EFIT data was not available before disruption. Again, the two-octant data was multiplied by a factor $\pi/2$ assuming a pure sine wave rotation in time. Both evaluations of the sideways impulse produce similar results, see figure 22.

It should be noted that since the asymmetry can rotate (see section 6) there is no direct relationship between the magnitude of the sideways impulse A (or Imp^F) and the ensuing sideways displacement of the vacuum vessel.

In general, there are three possible types of rotation.

(1) Trapped (or locked) mode in which the toroidal rotation can slow down and stay stationary during a significant time of the CQ.
(2) Non-resonant (slow) rotating mode, which rotates with a frequency below the vessel resonant frequency.
(3) Resonant mode which rotates near or above the resonant frequency of the vessel. Rotation at frequencies above the vessel resonant frequency can resonate with some mechanical components of the vessel.

It is worth mentioning, that provided it is not near a resonant frequency of the vessel, a rotating asymmetry will produce a lower sideways displacement than a (trapped) non-rotating asymmetry.

6. The rotation of plasma current asymmetries during disruptions in JET

6.1. Rotation numbers

The I_p asymmetry rotation is important since it can lead to the dynamic amplification of the applied force if resonance with the vessel or an in-vessel component occurs. In general for JET the duration of the rotation is short compared to resonance period of the vessel (~1/(14–17 Hz) [32]), and so dynamic amplification is not an issue. However in ITER the situation can be reversed (the duration of rotation is greater than the mechanical resonance period) making this an issue [16].

The I_p asymmetry rotation shows significant scatter in magnitude, frequency and direction [5, 8]. The 4-octant JET magnetic diagnostics allow the extraction of reliable information about I_p asymmetry toroidal rotation during disruptions. Figures 23, 24 and 25 show the asymmetrical disruption waveforms and the traces of the tip of vector $\delta\vec{I}_p(t) = (\delta I_{51}(t)\vec{e}_x + \delta I_{73}(t)\vec{e}_y)/I_p^{dis}$ for discharges with differing rotational behaviour. It can be seen that the rotation is highly variable and it is found that neighbouring pulses

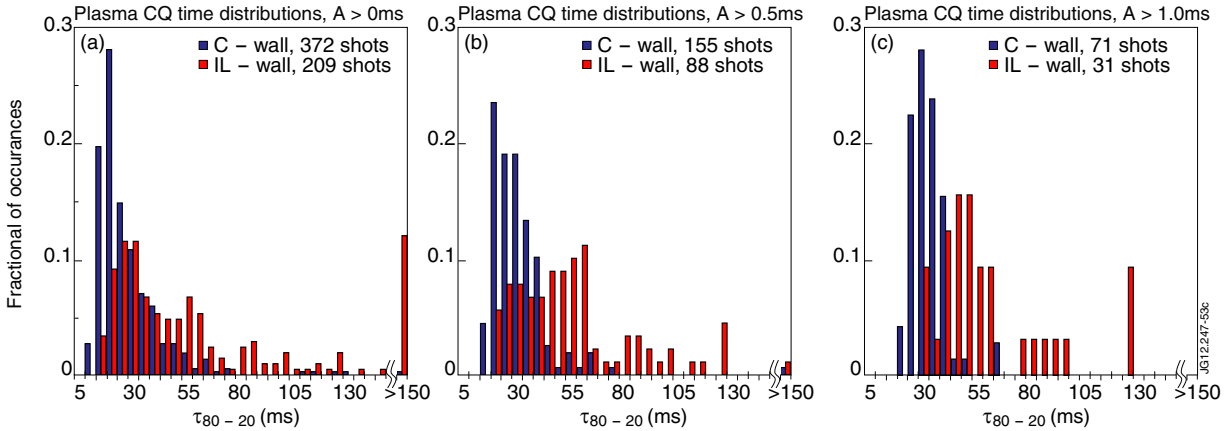

Figure 16. Plasma CQ time distributions for three thresholds of the I_p asymmetry integral (A) for C- and IL-walls.

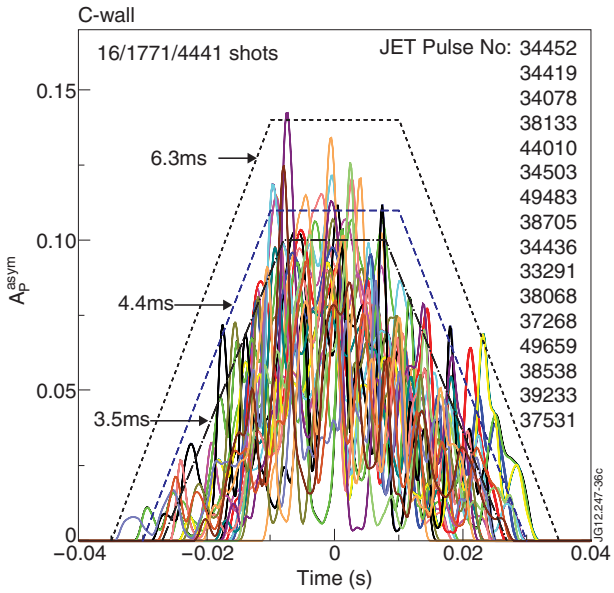

Figure 17. The smoothed normalized I_p asymmetries for 16 severest C-walls disruptions, where 1771/4441 is fraction of asymmetrical disruptions relative to whole C-wall database.

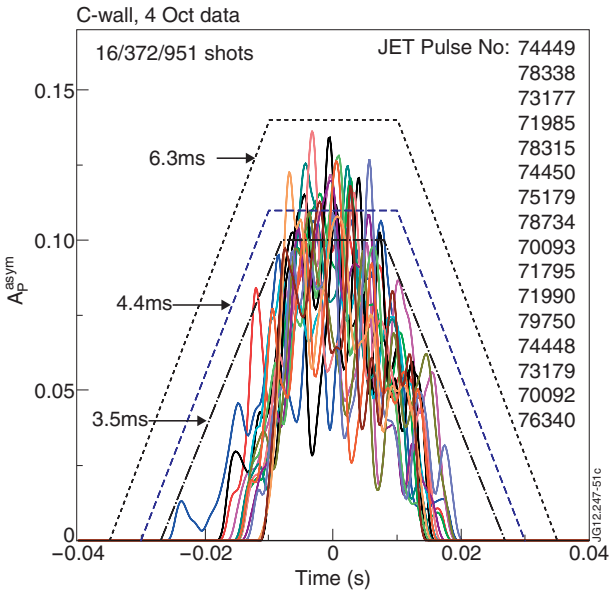

Figure 18. The smoothed normalized I_p asymmetries for 16 severest C-walls 4 octant data disruptions, where 372/951 is fraction of asymmetrical disruptions relative to C-wall 4 octant database.

(which are otherwise similar) show sometimes similar and sometimes very different rotational behaviour, figure 26. This strongly suggests the involvement of the plasma–wall interaction and current sharing in addition to plasma physics effects. However neighbouring pulses with similar asymmetry amplitude behaviour show similar rotational behaviour as well, see traces for pulses #70236 and #70238 on figure 26. At present there is no understanding of the rotational physics or appropriate scaling, though some models have been proposed [33].

The analysis of the rotational behaviour requires the use of criteria to extract a subset to avoid noise polluting the results; only shots satisfying $A = \int A_p^{asym}\,dt > 0.5$ ms have been used. The rotational shot set has been reduced from 951 to 155 shots for C-wall and from 349 to 88 shots for IL-wall. The number of rotation periods during a disruption was defined as $N = (\varphi_{max} - \varphi_{min})/2\pi$. The N distributions are very similar for C- and IL-walls, figure 27. However the mode rotation was slightly increased for the IL-wall. The N distributions are skewed, they are not normal, but for illustration purposes the mean ($\mu^N_{IL/C}$) and the standard deviation ($\sigma^N_{IL/C}$) are calculated: $\mu^N_{IL} = 2.1$ ($\sigma^N_{IL} = 1.2$) in comparison with the C-wall $\mu^N_C = 1.6$ ($\sigma^N_C = 0.8$). The rotation of the I_p asymmetry can be in either direction but it is most commonly seen in the electron drift direction (i.e. opposite to the plasma current direction) [8].

6.2. Rotation frequencies

An additional constraint has been applied for statistical analysis of the observed frequencies—analysis was only performed for pulses where the rotation exceeded one full turn during the disruption. As a result of this constraint, the total number of shots analysed for their frequency behaviour was reduced to 103 shots for C-wall and to 73 shots for IL-wall. The rotation frequency, presented in the current analysis, has been calculated as $f = 1/\tau$, where τ is the one turn period.

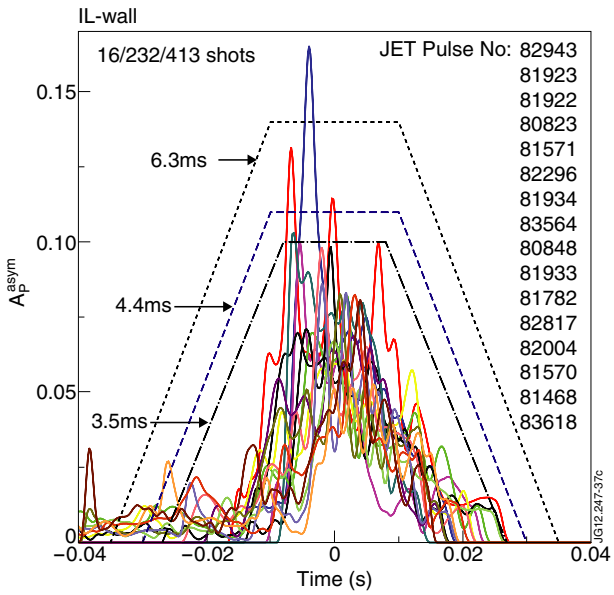

Figure 19. The smoothed normalized I_p asymmetries for 16 severest IL-walls disruptions, where 232/413 is fraction of asymmetrical disruptions relative to whole IL-wall database.

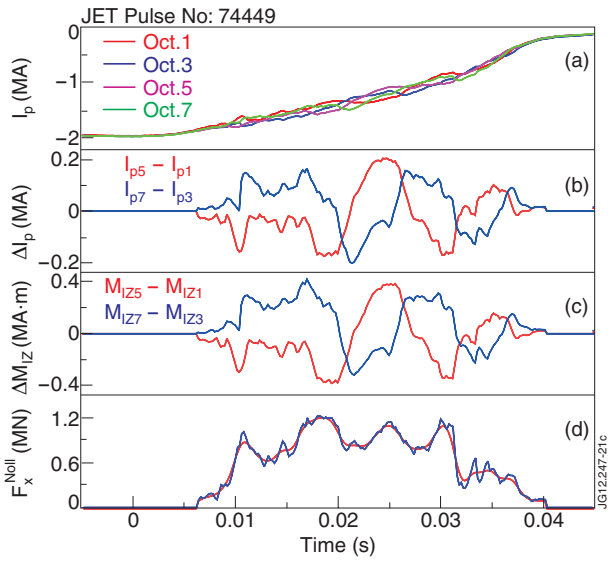

Figure 20. Waveforms of the measured asymmetries: (*a*) plasma currents, (*b*) I_p asymmetries, (*c*) M_{IZ} asymmetries, (*d*) F_x^{Noll} sideways force (blue—original, red—smoothed). The time axis is normalized to T_{dis}.

The average $\langle A_p^{asym} \rangle$ plasma current asymmetry amplitude has been calculated during the one period of rotation used to evaluate f. The above described algorithm has been applied to C- and IL-walls data independently.

Following this the data points were divided into five $\langle A_p^{asym} \rangle$ regions: $\langle A_p^{asym} \rangle < 2\%$, $2\% \leqslant \langle A_p^{asym} \rangle < 4\%$, $4\% \leqslant \langle A_p^{asym} \rangle < 6\%$, $6\% \leqslant \langle A_p^{asym} \rangle < 8\%$, $\langle A_p^{asym} \rangle \geqslant 8\%$. The means and the standard deviations of the distributions were calculated and plotted in figure 28, where error bars are the standard deviations. It can be seen that the rotation frequency does not decrease with I_p asymmetry amplitude.

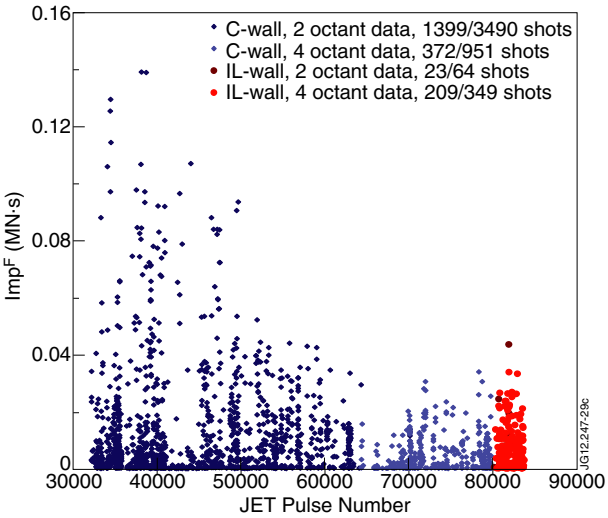

Figure 21. The sideways force impulse calculated using Noll's formula.

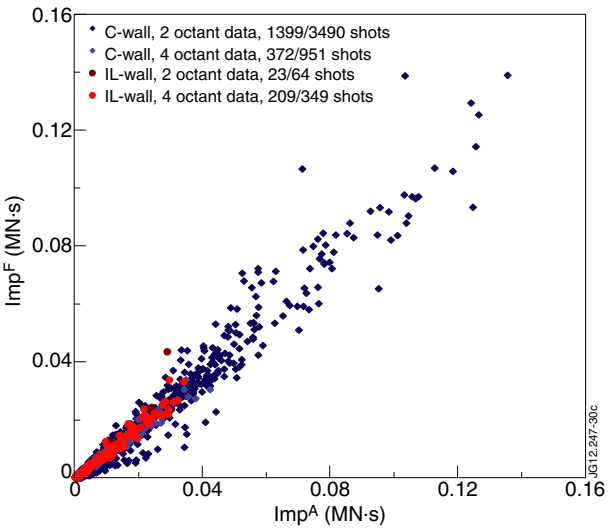

Figure 22. Relationship between sideways force impulse evaluated using the first current vertical moment (Imp^F) asymmetries and plasma current asymmetries (Imp^A).

7. Physical interpretation

In order to better understand the sideways forces one has to understand what physics leads to the plasma current asymmetries. The observed I_p asymmetries have been interpreted as an effect of the $m = n = 1$ kink mode, when the plasma boundary q-value decreases to about 1 to permit a kink instability [3, 17, 18].

Figure 2 illustrates the nature of the measured I_p asymmetries. Supposing the plasma is touching the wall in octant 7, during the kink mode $m = n = 1$ instability, a negative plasma surface current flows in the vessel in octant 7 and bypasses the contour of B_ϑ integration. In the opposite octant 3, the I_p diagnostic measures the total plasma current, as the plasma does not touch the wall.

The nature of the kink mode can explain the origin of the asymmetry. We consider a cylindrical plasma, with a circular cross-section, in a strong magnetic field and with

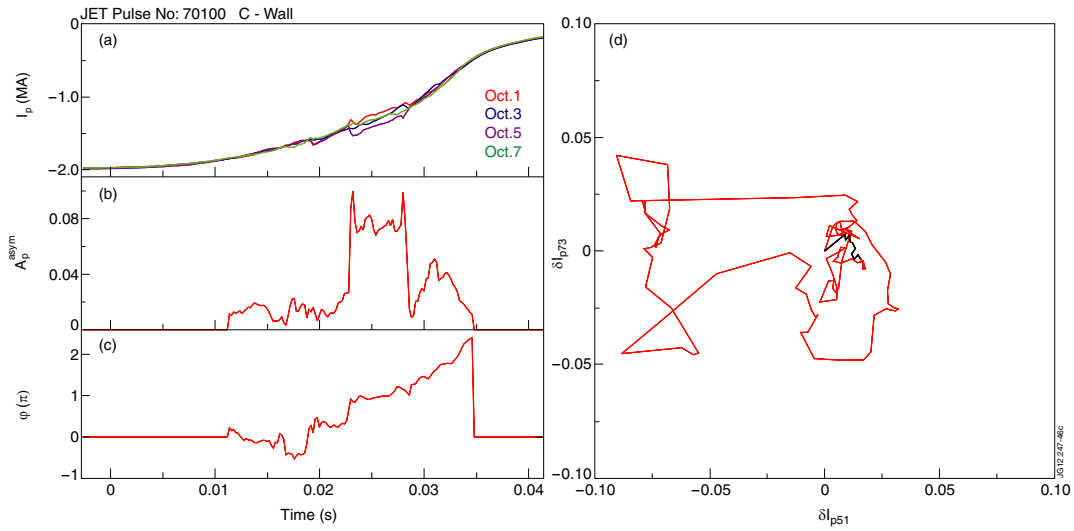

Figure 23. Example of the toroidally trapped motioned mode: (*a*) plasma currents, (*b*) normalized I_p asymmetry amplitude, (*c*) I_p asymmetry toroidal phase (φ) and (*d*) JET top view on trajectories of the tip of I_p asymmetry vector. The time axis is normalized to T_{dis}.

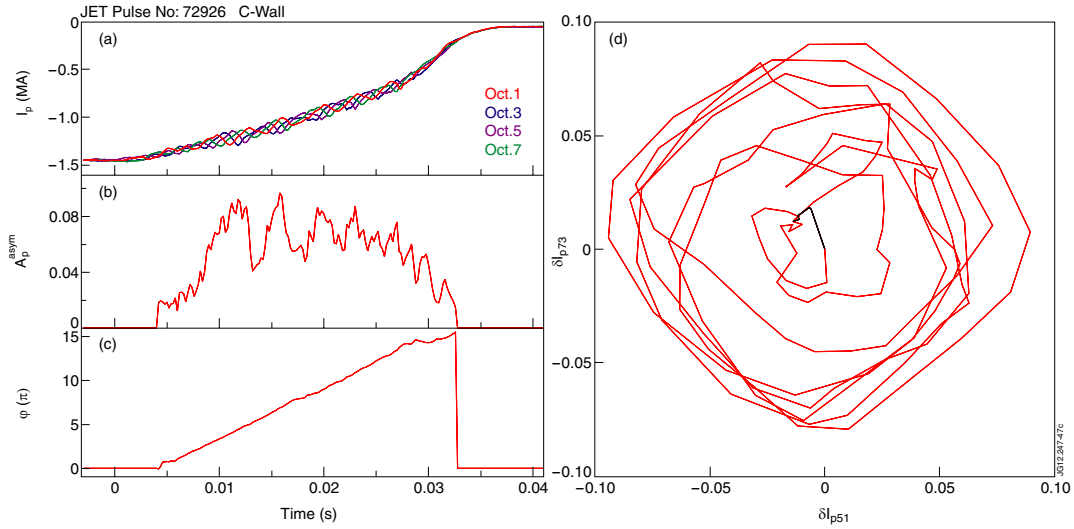

Figure 24. Example of the multi-turn fast rotation: (*a*) plasma currents, (*b*) normalized I_p asymmetry amplitude, (*c*) I_p asymmetry toroidal phase (φ) and (*d*) JET top view on trajectories of the tip of I_p asymmetry vector. The time axis is normalized to T_{dis}.

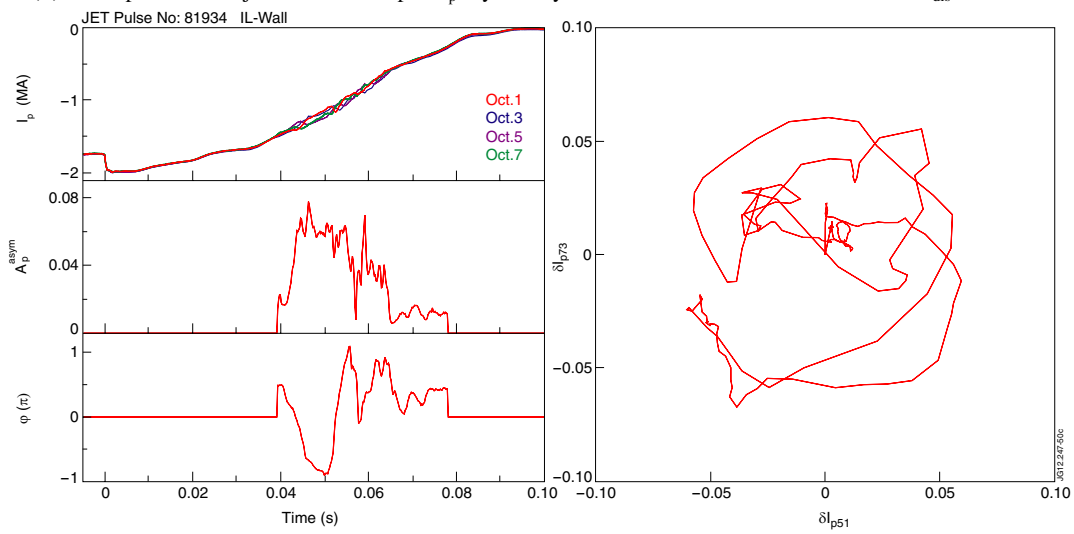

Figure 25. Example of rotation with reversal: (*a*) plasma currents, (*b*) normalized I_p asymmetry amplitude, (*c*) I_p asymmetry toroidal phase (φ) and (*d*) JET top view on trajectories of the tip of I_p asymmetry vector. The time axis is normalized to T_{dis}.

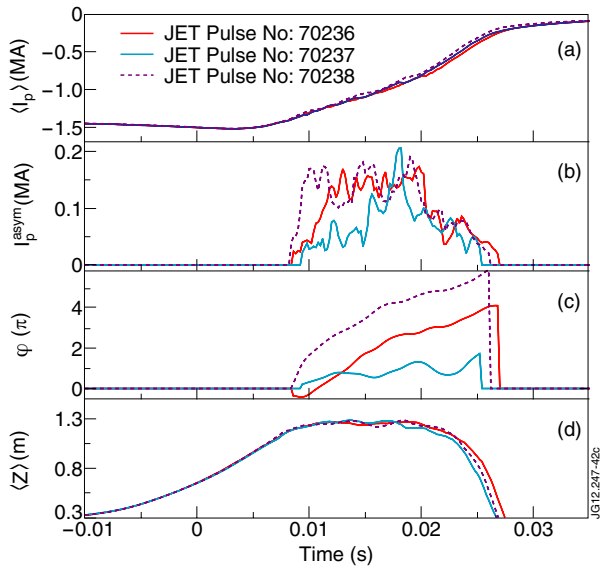

Figure 26. Examples of neighbouring pulses with similar plasma current and plasma current vertical displacement, in which (coincidentally) the earlier and the later pulses show coherent rotation and the intermediate pulse does not: (*a*) toroidally averaged plasma current $\langle I_p \rangle$, (*b*) I_p asymmetry amplitude, (*c*) I_p asymmetry toroidal phase (φ) and (*d*) toroidally averaged plasma current vertical centroid position $\langle Z \rangle$. The time axis is normalized to T_{dis}.

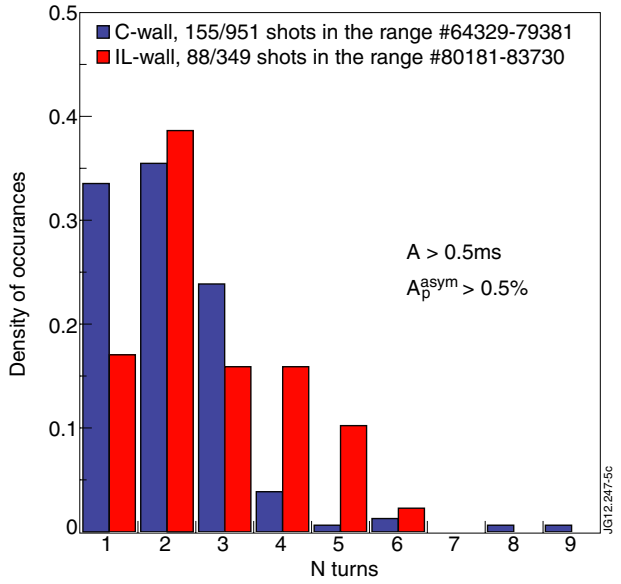

Figure 27. Distribution of the number of rotations.

plasma current (I_p) along the cylinder Z-axis (figure 29(*a*)). Allowing a kink mode deforms the straight cylindrical plasma to a helical structure. This helical deformation causes surface plasma currents in order to eliminate the normal component of the magnetic field on the plasma surface [18, 34]. The bulged-out surface always carries the negative current, opposite to I_p, whereas the bulged-in surface always carries the positive current. The important property of MHD instabilities is that the amplitude of the generated surface currents at the plasma boundary and currents in the wall is determined by the plasma deformation, rather than by its velocity, and the plasma instability acts as a current, rather than voltage, generator [7].

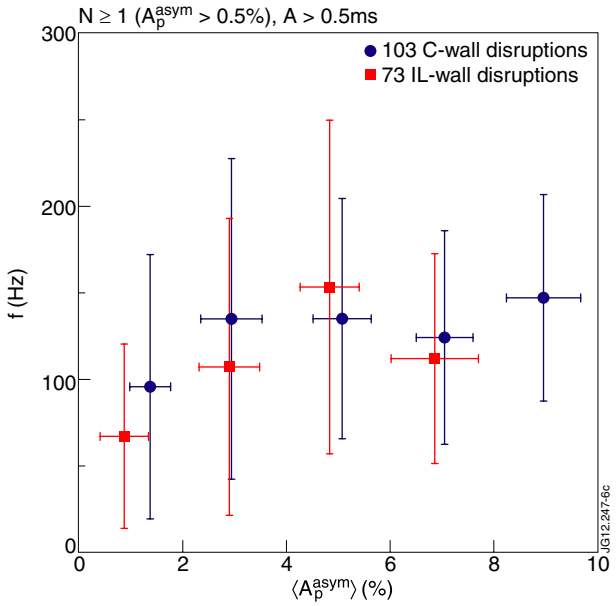

Figure 28. Variation of the 'one turn' frequency versus average I_p asymmetry amplitude.

This can be explained also from the electro-dynamic point of view, as described in detail in [7]. The edge localized currents are excited by the plasma motion with velocity V in the toroidal magnetic field B_T. In the case of the $m = 1$ motion (kink or vertical mode) the plasma carries its own magnetic field and it does not generate electromotive force (EMF) for the surface currents. They are generated by the component of the EMF $\vec{V} \times \vec{B}_T$ along the ignorable direction, which cannot be compensated by a scalar potential. Neglecting non-important resistive effects, which determine only the thickness of the plasma surface localized currents, the time derivative $\partial \vec{A}^{surf}/\partial t$ of their vector potential is equal to the driving EMF, which is proportional to V. As a result, the excited $\vec{A}^{surf}$ itself is determined by the plasma deformation, rather than by its velocity [18, 34].

However, the existence of the long lasting $m = n = 1$ kink mode contradicts the traditional interpretation of global kink mode behaviour [19]. A modern physically rooted model has been proposed based on the helical surface currents that occur in the kink mode [18]. The helical surface currents are assumed to flow into the wall when the kinking plasma surface touches the wall due to the kink mode, see figure 29(*b*). The model underlies the appearances of the plasma current asymmetries [7]. As was presented above the relative directions of the plasma motion and observed wall currents fit this model. Earlier, an empirical source and sink model has been proposed to explain forces, inferred from the vessel motion, by the observed I_p asymmetries [4]. This source and sink model has been used to calculate the structural loads from I_p asymmetries in ITER [9].

8. Outstanding issues

As discussed above the plasma current asymmetries could be associated with the $m = n = 1$ mode, and the vertical and radial displacements of the plasma boundary would be

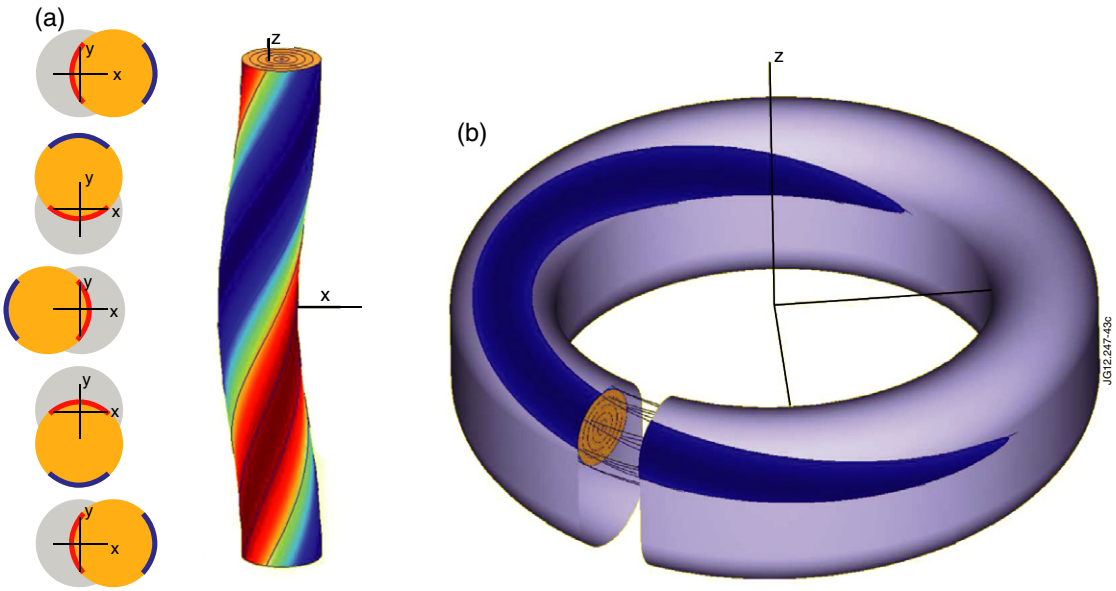

Figure 29. (*a*) The bulged-out surface always carries the negative (blue) current, opposite to I_p. The bulged-in surface always carries the positive (red) current. (*b*) Dark blue colour represents negative surfaces plasma current shared between vacuum vessel and plasma in VDE due to $m = n = 1$ kink mode.

expected to be approximately equal. However, the magnetic diagnostic shows a significantly lower first radial plasma current moment variation (ΔM_{IR}) compared with ΔM_{IZ}, figure 30. The reason of this is not yet determined. It is possible that the M_{IR} measurements are more strongly affected (screening effect) by plasma surface currents than M_{IZ} measurements. Another potential reason could be the effect of eddy currents in the wall, which is elongated in the vertical direction and, thus, better stabilize the radial displacement. We expect that numerical simulations with a realistic wall geometry and calibrated to the measurements can reveal the reason of the difference in M_{IZ} and M_{IR}.

A deeper analysis (Fourier decomposition) of MHD instabilities detected during disruptions is needed to support the relation between current asymmetries and (1,1) kink instability and to disclose other poloidal and toroidal harmonics.

The appropriate numerical model is also needed for the better evaluation of forces on the vessel. Noll's formula gives a good upper estimate of forces, but does not take into account the effect of eddy currents in the wall, which make the force a bit smaller. Such codes are not yet available and have to be created. The JET database gives exceptional opportunities for calibration of the numerical models.

The relationship of the poloidal halo current asymmetry (interpreted from B_T pick-up coil measurements) to the robust I_p asymmetry measurements in JET is discussed elsewhere [36, 37] and it is not yet fully resolved. There is a correlation between the I_p asymmetry and halo asymmetry, though with a large spread [37], but there is not a simple proportional relationship in amplitude. The understanding of poloidal halo currents on JET requires an appropriate physics model.

Understanding the reason why the toroidal motion of I_p asymmetries is sometimes rotational and sometimes sporadic is an outstanding issue.

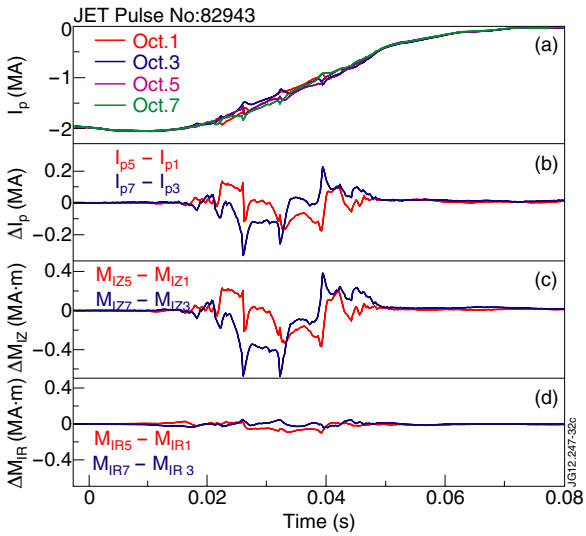

Figure 30. The magnetic diagnostic reported significantly lower first radial plasma current moment variation (ΔM_{IR}) compare with ΔM_{IZ}. (*a*) plasma currents, (*b*) I_p asymmetries, (*c*) M_{IZ} asymmetries, (*d*) M_{IR} asymmetries. The time axis is normalized to T_{dis}.

9. Summary and discussion

The JET disruption data shows toroidal asymmetries in I_p that can translate into substantial sideways forces on the vacuum vessel. These asymmetries have a dominantly $n = 1$ structure and probably arise from a $m = n = 1$ kink mode, though a full comparison with an appropriate simulation is needed to unambiguously establish this.

The present JET database includes 4854 disruptions over an 18 year period. For fairly recent shots around 1300 are available with data in 4 toroidally orthogonal octants, allowing the phase and amplitude to be deduced. Previously only 2

toroidally opposite octants of data were regularly recorded. The amplitude (smoothed, peak to peak) of the I_p asymmetries is $\leqslant$17% of pre-disruptive I_p and the severest asymmetries have an average CQ duration of ~30 ms for C-wall disruptions (from #64329 onwards) and two times longer for IL-walls. The plasma current quench time is significantly increased for IL-wall compared with C-wall disruptions. In spite of this, the observed I_p toroidal asymmetry time integral, $A \sim$ sideways force impulse, did not increase for IL-wall disruptions and remained inside the C-wall data domain if $A < 3.5$ ms. Due to the observed I_p toroidal asymmetry rotation, the sideways displacement cannot be directly linked with the magnitude of the sideways impulse (A)—the relationship of the I_p asymmetries and sideways vessel displacements will be the subject of a future publication.

A trapezoidal shaped envelope for A_p^{asym} with a 3.5 ms area, does not contain all of the observed waveforms. A conservative choice would be 4.4 ms and a very conservative choice would be 6.3 ms for C- and IL-wall disruptions.

Although not discussed in this paper, the effect of massive gas injection (MGI) on the I_p asymmetries has been examined [27]. It is found the MGI reduces the I_p asymmetries by an order of magnitude, substantially ameliorating the problem.

The rotation of the I_p asymmetry during the I_p quench has a quite variable behaviour and is not reproducible on a shot-by-shot basis. There is no confirmed understanding of the rotational physics or appropriate scaling at present. Distributions of the number of rotation periods are very similar for both C- and IL-wall disruptions, while multi-turn mode rotations were observed in some cases. For both C- and IL-walls, the amplitude of the I_p toroidal asymmetry does not degrade with the mode rotation frequency. This fact indicates that the dynamic amplification of the forces on the vessel by the mechanical resonance of machine components with the multi-turn I_p asymmetry rotation remains a serious issue.

Acknowledgments

The authors would like to acknowledge M.F. Johnson for initial development of the JET disruption database and P. Noll for helpful discussions. This work, part-funded by the European Communities under the contract of Association between EURATOM/CCFE was carried out within the framework of the European Fusion Development Agreement. For further information on the contents of this paper please contact publications-officer@jet.efda.org. The views and opinions expressed herein do not necessarily reflect those of the European Commission. This work was also partially funded by the RCUK Energy Programme (grant number EP/I501045) and by the US DoE contract No DE-AC02-09-CH11466.

References

[1] Hender T.C. *et al* 2007 Progress in the ITER Physics Basis: chapter 3. MHD stability, operational limits and disruptions *Nucl. Fusion* **47** S128–202 (beginning of chapter)
[2] Sugihara M. *et al* 2007 *Nucl. Fusion* **47** 337
[3] Noll P. *et al* 1996 *Proc. 19th Symp. on Fusion Technology (Lisbon, Portugal, 1996)* vol 1 p 751 www.iop.org/Jet/fulltext/JETP96044.pdf
[4] Riccardo V. *et al* 2000 *Nucl. Fusion* **40** 1805
[5] Gerasimov S.N. *et al* 2010 *European Physical Society Conf. on Plasma Physics (Dublin, Ireland, 2010)* P4.121 http://ocs.ciemat.es/EPS2010PAP/pdf/P4.121.pdf
[6] Hender T.C. 2010 *Proc. 23rd Int. Conf. on Fusion Energy 2010 (Daejeon, Korea, 2010)* (Vienna: IAEA) CD-ROM file EXS/10-3 and www-naweb.iaea.org/napc/physics/FEC/FEC2010/index.htm
[7] Zakharov L.E. *et al* 2012 *Phys. Plasmas* **19** 055703
[8] Gerasimov S.N. *et al* 2012 *European Physical Society Conf. on Plasma Physics (Stockholm, Sweden, 2012)* P5.074 ocs.ciemat.es/epsicpp2012pap/pdf/P5.074.pdf
[9] Bachmann C. *et al* 2011 *Fusion Eng. Des.* **86** 1915
[10] Neyatani Y., Yoshino R. and Ando T. 1995 *Fusion Technol.* **28** 1634
[11] Granetz R.S. *et al* 1996 *Nucl. Fusion* **36** 545
[12] Evans T.E. *et al* 1997 *J. Nucl. Mater.* **241–243** 606
[13] Pautasso G. *et al* 2011*Nucl. Fusion* **51** 043010
[14] Gerhardt S.P. *et al* 2012 *Nucl. Fusion* **52** 063005
[15] Gerhardt S.P. *et al* 2013 *Nucl. Fusion* **53** 023005
[16] Schioler T. *et al* 2011 *Fusion Eng. Des.* **86** 1963
[17] Manickam J., Boozer A. and Gerhardt S. 2012 *Phys. Plasmas* **19** 082103
[18] Zakharov L. 2008 *Phys. Plasmas* **15** 062507
[19] Shafranov V.D. 1970 *Sov. Phys.—Tech. Phys.* **15** 175
[20] Zakharov L.E. and Shafranov V.D. 1986 *Reviews of Plasma Physics* vol 11, ed M.A. Leontovich (New York: Consultants Bureau) p 153
[21] Pick M.A. *et al* 1989 *15th SOFT 1988 (Amsterdam, The Netherlands, 1989*) vol 1, p 776 ISBN: 0444 873694
[22] DeVries P.C. *et al* 2012 *Plasma Phys. Control. Fusion* **54** 124032
[23] Brezinsek S. *et al* 2013 *Nucl. Fusion* **53** 083023
[24] Riccardo V. *et al* 2013 *27th Symp. on Fusion Technology (SOFT-2012) (Liege, Belgium, 2013) Fusion Eng. Design* **88** 585–9
[25] Romanelli F. *et al* 2012 *Proc. 24th Int. Conf. on Fusion Energy (San Diego, CA, 2012)* www-naweb.iaea.org/napc/physics/FEC/FEC2012/index.htm
[26] Strauss H.R. *et al* 2010 *Phys. Plasmas* **17** 082505
[27] Lehnen M. *et al 2013 Nucl. Fusion* **53** 093007
[28] Bachmann C. 2009 *ITER Report* ITER_D_2DJ5AA v 2.7 https://user.iter.org/?uid=2DJ5AA
[29] Harris G.R. 1990 Comparisons of the current decay during carbon-bounded and beryllium bounded disruptions in JET JET-R (90) 07 www.iop.org/Jet/fulltext/JETR90007.pdf
[30] McGrath R.T. and Kellman A.G. 1992 *Nucl. Fusion* **32** 2054
[31] Granetz R.S. *et al* 2007 *Nucl. Fusion* **47** 1086
[32] Last J. *et al* 1999 Raising the JET Toroidal Field to 4 Tesla *JET-R (99) 10* www.iop.org/Jet/fulltext/JETR99010.pdf
[33] Boozer A.H. 2012 *Phys. Plasmas* **19** 052508
[34] Zakharov L.E. 2011 *Phys. Plasmas* **18** 062503
[35] Boozer A.H. 2012 *Phys. Plasmas* **19** 058101
[36] Riccardo V. *et al* 2010 *Plasma Phys. Control. Fusion* **52** 124018
[37] Hender T.C. *et al* 2011 Report of the ITPA MHD Working Group 6 on Non-Axisymmetric Currents During VDEs EFDA–JET–R(11)01 www.iop.org/Jet/fulltext/EFDR11001.pdf